

Article

Insight into the Acidity and Catalytic Performance on Butane Isomerization of Thermal Stable Sulfated Monoclinic Zirconia

Daofeng Huang, Wenhua Feng, Li Zhang, Bin Yue * and Heyong He *

Department of Chemistry and Shanghai Key Laboratory of Molecular Catalysis and Innovative Materials, Fudan University, Shanghai 200438, China

* Correspondence: yuebin@fudan.edu.cn (B.Y.); heyonghe@fudan.edu.cn (H.H.); Tel.: +86-21-3124-3916 (H.H.); Fax: +86-21-3124-5572 (H.H.)

Abstract: Sulfated monoclinic zirconia (M-SZ) with high thermal stability and high catalytic performance on butane isomerization were obtained by hydrothermal method followed with sulfation treatment. The acidity of M-SZ was studied by ^{31}P MAS NMR, with trimethylphosphine (TMP) as the probe molecule, and the catalytic performance of 1- ^{13}C -*n*-butane over M-SZ was monitored by ^{13}C MAS NMR spectroscopy. Both Brønsted and Lewis acids were observed on M-SZ. Only Brønsted acid strength shows close relation to the activation energy of butane isomerization, and the M-SZ catalyst with the strongest Brønsted acid strength shows the lowest activation energy of $46.4\text{ kJ}\cdot\text{mol}^{-1}$. The catalytic stability tests were evaluated at 673 K for 240 h, which shows that sulfated monoclinic zirconia has higher thermal stability than sulfated tetragonal zirconia.

Keywords: monoclinic; sulfated zirconia; butane isomerization; solid-state NMR



Citation: Huang, D.; Feng, W.; Zhang, L.; Yue, B.; He, H. Insight into the Acidity and Catalytic Performance on Butane Isomerization of Thermal Stable Sulfated Monoclinic Zirconia. *Processes* **2022**, *10*, 2693. <https://doi.org/10.3390/pr10122693>

Academic Editor: Blaž Likozar

Received: 15 November 2022

Accepted: 8 December 2022

Published: 13 December 2022

Publisher's Note: MDPI stays neutral with regard to jurisdictional claims in published maps and institutional affiliations.



Copyright: © 2022 by the authors. Licensee MDPI, Basel, Switzerland. This article is an open access article distributed under the terms and conditions of the Creative Commons Attribution (CC BY) license (<https://creativecommons.org/licenses/by/4.0/>).

1. Introduction

With the reduction in fossil energy reserves, promoting resource efficiency has become an important topic in current catalysis research. Isomerization of paraffin can convert straight-chain paraffin into higher-value branched-chain paraffin, which is an effective way to improve resource utilization efficiency [1]. As the product of butane isomerization, isobutane is an important feedstock for the additive MTEB used to enhance gasoline octane number of synthetic gasoline. Much progress has been made in the development of industrial catalysts for butane isomerization, such as Pt/Al₂O₃-Cl, Pt-MOR, and sulfated oxide catalysts [2–4]. As an important catalyst with high catalytic performance, sulfated zirconia has been widely studied because of its super acidity, which is of great potential in the butane isomerization reaction [5–8].

It is generally believed that sulfated tetragonal zirconia has super acidity, while the acidic strength of sulfated monoclinic zirconia is relatively low [9]. Therefore, researchers mainly focus on the in-depth understanding of the structure and catalytic properties of sulfated tetragonal zirconia [9,10] and pay much less attention to monoclinic zirconia sulfation. Stichert et al. compared the monoclinic and tetragonal sulfated zirconia in catalyzing butane isomerization [11]. It was found that both phases of sulfated zirconia are catalytically active in the butane isomerization reaction, indicating that the sulfated monoclinic zirconia can also act as an acid catalyst. They also studied the surface acidity of sulfated monoclinic and tetragonal zirconia by adsorption of CO [12] and found similar acid strength of the two catalysts. However, the catalytic performance for butane isomerization of sulfated monoclinic zirconia is about 25% of that of sulfated tetragonal zirconia. Zhang et al. studied the dehydration cyclization reaction of sorbitol on sulfated zirconia catalysts prepared from zirconium hydroxide, tetragonal zirconia, and monoclinic zirconia [13]. The results showed that the catalytic performance of sulfated tetragonal synthesized from zirconium hydroxide was significantly higher than those prepared from tetragonal and monoclinic zirconia. Meanwhile, the catalytic performance of sulfated monoclinic zirconia obtained

from monoclinic zirconia is higher than that of sulfated tetragonal zirconia synthesized from tetragonal zirconia. In addition, the thermodynamic stability of the monoclinic phase (<1448 K) is significantly higher than that of the tetragonal phase [14], so the zirconia could undergo a tetragonal-to-monoclinic phase transformation at high catalytic reaction temperatures. Therefore, the research on sulfated monoclinic zirconia may expand the types of sulfated zirconia superacid catalysts, leading to a deeper exploring of highly thermal stable sulfated zirconia catalysts.

Magic-angle spinning solid-state nuclear magnetic resonance (MAS NMR) is widely used in characterizing the surface acidity of the catalysts, and it is also a useful tool to analyze surface catalytic reactions. On the one hand, the surface acidity of the catalysts may be studied by directly detecting the hydroxy group with ^1H NMR [15,16] or characterizing the probe molecules adsorbed on the catalyst, such as ^{31}P , ^{13}C , and ^{15}N NMR spectroscopies with trimethylphosphine (TMP) or trimethylphosphine oxide (TMPO) [17,18], ^{13}C -acetone [19], and ^{15}N -pyridine [20] as probe molecules, respectively. On the other hand, solid-state NMR spectroscopy using isotopically labeled reaction molecules may monitor the evolution of related molecules during the reaction and study the catalytic reaction mechanism [21,22].

In this paper, a series of monoclinic zirconia and their sulfated counterparts were prepared. The catalytic reaction was studied by ^{13}C MAS NMR, with 1- ^{13}C -*n*-butane as the reactant. The surface acidity of the catalyst was characterized by ^{31}P MAS NMR, using TMP as the probe molecule. The effect of surface acidity on the butane isomerization reaction was studied.

2. Materials and Methods

2.1. Preparation of the Samples

Monoclinic zirconia (M-ZrO₂) was prepared by the hydrothermal method. Typically, 9.25 g of zirconyl nitrate hydrate (ZrO(NO₃)₂·xH₂O, 99.5%, Shanghai Aladdin Biochemical Technology Co., Ltd., Shanghai, China) and 4.80~28.81 g of urea (CO(NH₂)₂, 99%, Sigma-Aldrich, Co., Saint Louis, MO, USA) were dissolved in 100 mL of deionized water. The solution was then poured into a 200 mL Teflon-lined stainless steel autoclave was treated at different temperatures (393, 433, and 473 K) for 12 h. The obtained white solid was washed with deionized water, separated by centrifugation, and dried at 393 K overnight. It was then calcined in static air with a heating rate of 2 K min⁻¹ to 673 K for 4 h in a tube furnace. Sulfated zirconia was prepared by the impregnation method. A total of 1 g of monoclinic zirconia was dispersed in 15 mL of 1 mol·L⁻¹ H₂SO₄ solution, stirred for 30 min at room temperature, and, finally, filtered and dried at 393 K. The white solid was put into a tube furnace and calcined in static air at 823 K for 3 h with 5 K min⁻¹ rate. Among the synthesized monoclinic zirconia samples, as shown in Figure S1, three samples with Zr:Urea molar ratio of 1:12, 1:6, and 1:2 were selected for the following study and named as M-ZrO₂-1, M-ZrO₂-2, and M-ZrO₂-3, and their sulfated counterparts were named as M-SZ-1, M-SZ-2, and M-SZ-3, respectively. For M-ZrO₂-1, 28.81 g of urea was used, and the hydrothermal temperature was 393 K. For M-ZrO₂-2, 14.40 g of urea was used, and the hydrothermal temperature was 433 K. For M-ZrO₂-3, 4.80 g of urea was used, and the hydrothermal temperature was 473 K. In addition, another sample, M-SZ-4, was prepared by sulfation using M-ZrO₂-2 as the precursor, and 2 mol·L⁻¹ H₂SO₄ solution was used instead of 1 mol·L⁻¹ H₂SO₄ solution.

Tetragonal zirconia was prepared by the precipitation method [23]. A total of 24.17 g of zirconyl chloride octahydrate (ZrOCl₂·8H₂O, 99%, Shanghai Aladdin Biochemical Technology Co., Ltd., Shanghai, China) was dissolved into 150 mL of deionized water, and 50 mL of ammonia solution (NH₃·H₂O 14.8 mol·L⁻¹, Sinopharm Chemical Reagent Co., Ltd., Shanghai, China) was then dropped into the zirconium solution at a rate of 30 mL·h⁻¹. The mixture was stirred at room temperature for 48 h. Using deionized water as the washing reagent, the white sample was washed and filtrated three times. After drying at 393 K overnight, the sample was put into the tube furnace and calcined under air at 673 K for

3 h with $5 \text{ K}\cdot\text{min}^{-1}$ rate. A total of 1 g of $\text{Zr}(\text{OH})_4$ was sulfated in a similar process to the sulfation of M-ZrO_2 at a calcination temperature of 873 K. The obtained white powder was named as T-SZ-general.

2.2. Characterization of the Catalysts

X-ray diffraction (XRD) patterns were obtained on a Bruker D2 PHASER diffractometer. The $\text{Cu-K}\alpha$ radiation was used ($\lambda = 0.15418 \text{ nm}$) at the voltage of 30 kV and the current of 10 mA. The range of 2θ was from 10° to 80° and the step width was 0.02° , while the step time was 0.2 s.

Fourier transform infrared (FT-IR) spectra were recorded on a Nicolet iS 10 infrared spectrometer from Thermo Fisher Scientific (Waltham, MA, USA). The detection range is from 400 to 4000 cm^{-1} . The sample was dispersed in KBr and pressed into a disc before the detection.

X-ray photoelectron spectra were collected using a PHI 5000C ESCA spectrometer from PerkinElmer (Waltham, MA, USA). The source was monochromatic $\text{Mg K}\alpha$ radiation (1253.6 eV) with the voltage of 14 kV and the current of 20 mA. The banding energy of all elements was calibrated by C 1s of the contaminated carbon at 284.8 eV .

The microstructure images of the samples were collected on an FEI Tecnai Ge F20 S-Twin transmission electron microscope (TEM). The samples were dispersed in ethanol by ultrasonic for 600 s, and the suspensions were dripped onto copper grids coated with carbon film.

The N_2 adsorption–desorption isotherms were obtained with a Micromeritics Tristar II 3020 porosimetry analyzer at 77 K. Before the measurement, the samples were treated at 573 K for 2 h to remove physically adsorbed gases before the measurement. The specific surface areas of the samples were calculated by Brunauer–Emmett–Teller (BET) equation. The cumulative pore volumes and average pore diameters were calculated from the desorption branch of the isotherms by the Barrett–Joyner–Halenda (BJH) model.

For the ^{31}P MAS NMR experiments, an appropriate amount ($0.15 \sim 0.20 \text{ g}$) of catalyst was put into a glass tube, shown in Figure S2b. The tube was connected to a vacuum system and evacuated to about $1\sim 2 \text{ Pa}$. The samples were then heated to 573 K at a heating rate of $10 \text{ K}\cdot\text{min}^{-1}$ and kept for 2 h. The TMP probe molecules were adsorbed onto the catalyst through a vacuum system, and the amounts of the probe molecules adsorbed on the samples were controlled by the pressure change. The glass sample tube with the sample was sealed by flame and transferred to the glove box, which is filled with high-purity nitrogen. The sample was then packed into 4 mm zirconia rotors with Kel-F caps in the glove box. Using a Bruker ADVANCE III 400 WB spectrometer, the MAS NMR spectra were recorded. The resonance frequency of ^{31}P was 161.9 MHz to be consistent with the nucleus, and 85 wt% H_3PO_4 was used as the external standard. ^1H high-power decoupling and one-pulse ^{31}P MAS NMR experiments were conducted at 12 kHz magic angle speed, $1.1 \mu\text{s}$ pulse width (30° pulse), 15 s relaxation delay time, and 120 to 960 scans.

2.3. Solid-State NMR Study on Isomerization of $1\text{-}^{13}\text{C}\text{-}n\text{-Butane}$

An appropriate amount of catalyst ($50\sim 100 \text{ mg}$) was put into a glass tube, which can be well-matched with a 7 mm NMR rotor (Figure S2c). Similar to the pretreatment of the sample in Section 2.2, $400 \mu\text{mol}\cdot\text{g}^{-1}$ of $1\text{-}^{13}\text{C}\text{-}n\text{-butane}$ was introduced at liquid nitrogen temperature. Then, the glass tube with the catalyst was protected in liquid nitrogen and symmetrically flame-sealed for achieving the desirable MAS speed, as shown in Figure S2. In the NMR study, the sealed glass sample tube was heated in a tube furnace at a desirable reaction temperature for a certain time and then put into the liquid nitrogen to quench the reaction. The ^{13}C MAS NMR spectra were acquired by Bruker ADVANCE III 400 WB spectrometer at 100.7 MHz using tetramethylsilane (TMS) as the external standard. ^1H high-power decoupling ^{13}C MAS NMR experiments were conducted at ca. 1 kHz MAS speed, $1.2 \mu\text{s}$ pulse width (30° pulse), 8 s relaxation delay time, and 120 to 360 scans.

The content of reactant or product ($C_{i,t}$) at time t is:

$$C_{i,t} = \frac{I_{i,t}}{\sum I_{i,0}} \times 100\%$$

In this equation, $I_{i,0}$ represents the peak area of the reactant and the products in the original NMR spectrum. $I_{i,t}$ is the peak area of the reactant and the products after reacting for t min. The conversion of 1- ^{13}C - n -butane after reacting for t min was calculated as:

$$X_t = 1 - C_{a,t} \text{ (a represents 1-}^{13}\text{C-}n\text{-butane)}$$

3. Results and Discussion

3.1. Characterization

The XRD patterns of M-ZrO₂-1, M-ZrO₂-2, M-ZrO₂-3, M-SZ-1, M-SZ-2, and M-SZ-3 are shown in Figure 1a. The diffraction peaks at 28.2° and 31.5° correspond to (-111) and (111) planes of monoclinic zirconia (JCPDS No. 37-1484). The results show that the sulfation only decreases the full width at half maximum (FWHM) of the peaks, indicating the unchanged crystal phase and the increase in particle size after the sulfation. The FT-IR spectra in Figure 1b show that M-SZ-1, M-SZ-2, and M-SZ-3 have distinct characteristic bands at 1232, 1132, 1042, and 993 cm⁻¹, where the first two bands correspond to S=O asymmetry and symmetric stretching vibrations and the latter two bands correspond to the asymmetric and symmetric stretching vibrations of S-O, indicating that the M-ZrO₂-1, M-ZrO₂-2, and M-ZrO₂-3 samples were successfully sulfated.

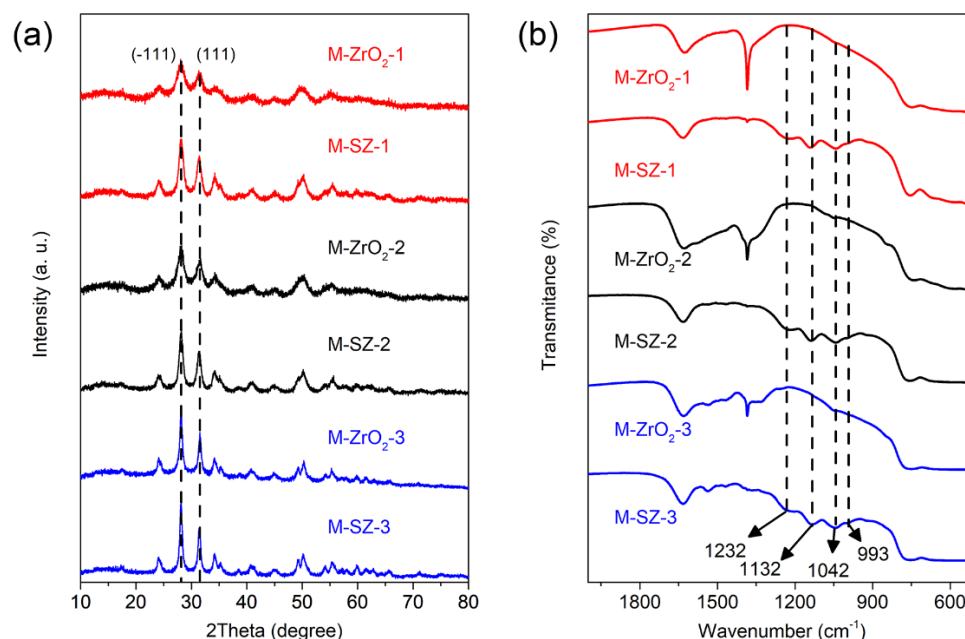


Figure 1. (a) The XRD patterns and (b) FT-IR spectra of M-ZrO₂-1, M-SZ-1, M-ZrO₂-2, M-SZ-2, M-ZrO₂-3, and M-SZ-3.

The XPS spectra of zirconia and their sulfated counterparts are shown in Figure 2. The peaks near 530.8 eV in M-ZrO₂ correspond to the O 1s electrons of the oxygen ions in zirconia, while the peaks near 532.2 eV are related to the oxygen ions affected by sulfation [24]. The peaks near 182.6 and 185.0 eV are related to the Zr 3d_{5/2} and Zr 3d_{3/2} electrons of the tetravalent-state zirconium ions in zirconia [25]. All XPS peaks of zirconia, as well as sulfated zirconia, indicate no noticeable change in the chemical environment of oxygen ions and zirconium ions.

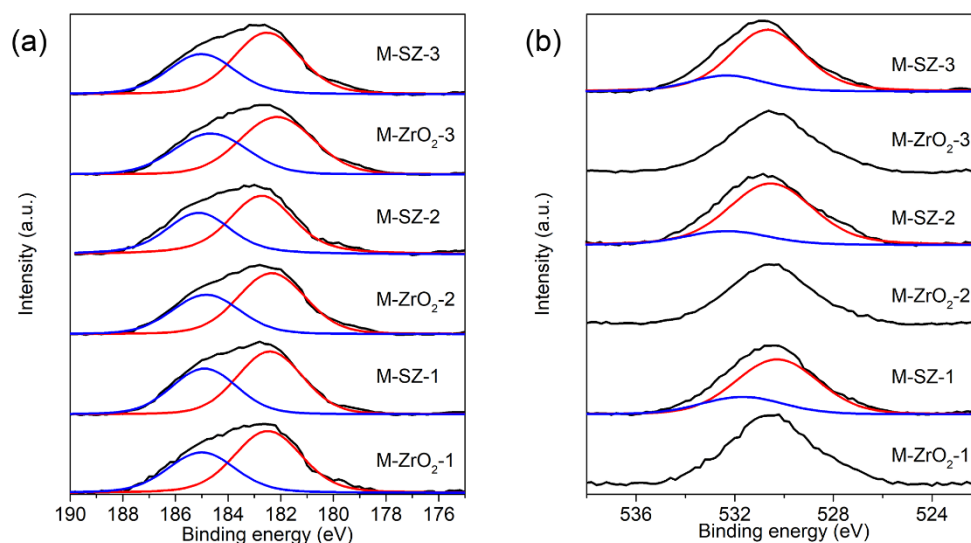


Figure 2. (a) Zr 3d and (b) O 1s XPS spectra of M-ZrO₂-1, M-ZrO₂-2, M-ZrO₂-3, M-SZ-1, M-SZ-2, and M-SZ-3.

Figure 3 displays the TEM images of three monoclinic zirconia and their sulfated catalysts. All three samples contain irregular pore structures. Compared with M-ZrO₂, no significant changes were observed in the morphology and pore structure.

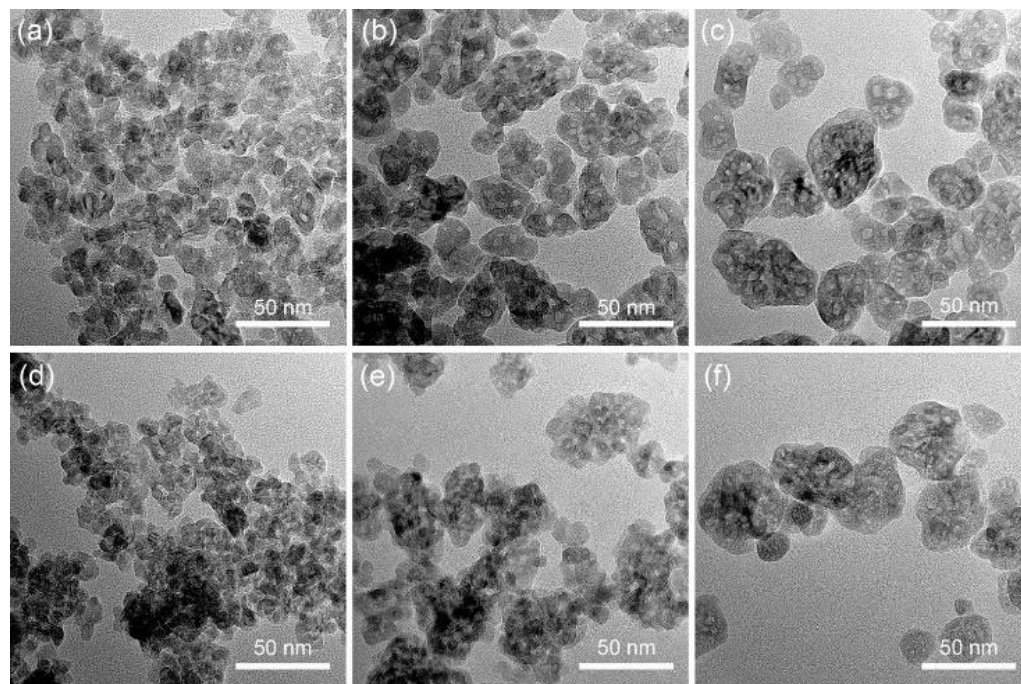


Figure 3. The TEM image of (a) M-ZrO₂-1, (b) M-ZrO₂-2, (c) M-ZrO₂-3, (d) M-SZ-1, (e) M-SZ-2, and (f) M-SZ-3.

The N₂ adsorption–desorption isotherms and pore size distributions of the samples are shown in Figure 4. The isotherms are type IV with H1 hysteresis loops, indicating that the samples have mesoporous structures. The results related to the texture properties are shown in Table 1. After the calcination in sulfation, all three sulfated zirconia samples decrease significantly in their specific surface area and increase in the pore volume and pore size.

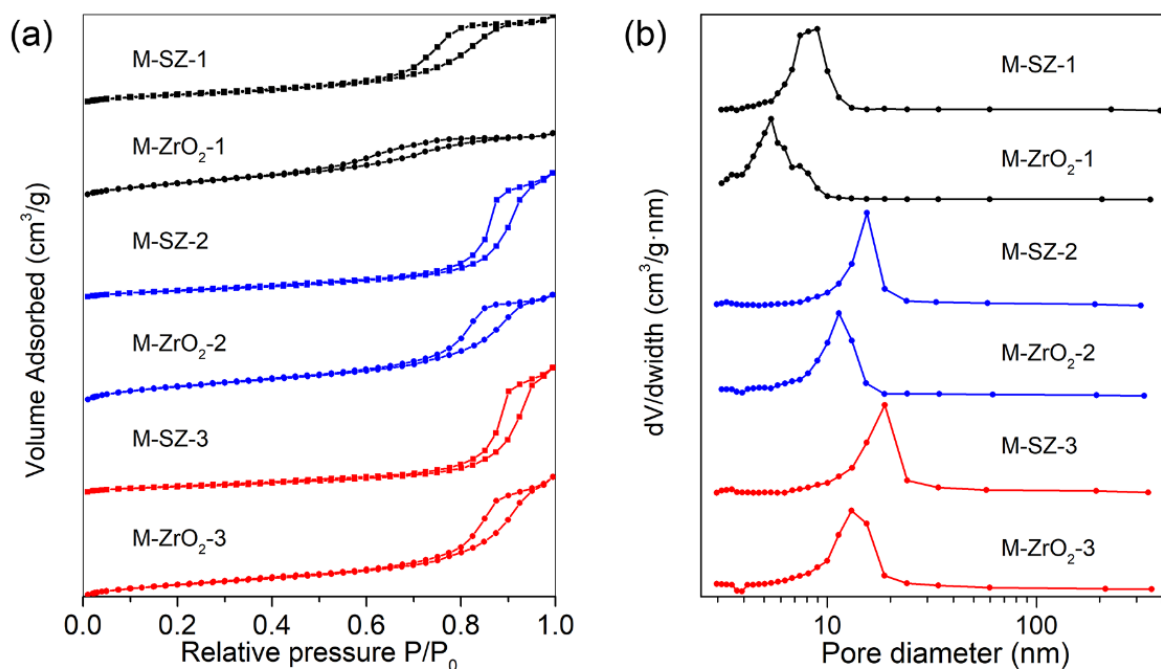


Figure 4. (a) N_2 adsorption–desorption isotherms and (b) pore distribution of M-ZrO₂-1, M-ZrO₂-2, M-ZrO₂-3, M-SZ-1, M-SZ-2, and M-SZ-3.

Table 1. The specific surface area, pore volume, and pore diameter of the samples.

Samples	BET Surface Area (m ² ·g ⁻¹)	Pore Volume (cm ³ ·g ⁻¹)	Average Pore Diameter (nm)
M-ZrO ₂ -1	119	0.129	5.4
M-SZ-1	76	0.195	7.4
M-ZrO ₂ -2	169	0.213	11.4
M-SZ-2	67	0.265	15.5
M-ZrO ₂ -3	136	0.246	13.1
M-SZ-3	57	0.263	18.8

Figure 5a illustrates the ¹H-decoupled ³¹P MAS NMR spectra of three sulfated zirconia after adsorption of TMP, and the relevant results are listed in Table 2. The peaks in the range of 0~−7 ppm are related to TMP adsorbed on Brønsted acid sites (BA), and those between −20 and 60 ppm correspond to TMP adsorbed on Lewis acid sites (LA) [26]. The ³¹P chemical shifts of the peaks related to BA on M-SZ-1, M-SZ-2, and M-SZ-3 are −3.4, −3.2, and −3.3 ppm, which reflect the BA acid strength being in the order of M-SZ-2 > M-SZ-3 > M-SZ-1. However, it is worth mentioning that a large change in the BA acid strength only corresponds to a relatively narrow change in ³¹P chemical shifts of adsorbed TMP [27]. Therefore, the ³¹P chemical shift of adsorbed TMP on M-SZ-1, M-SZ-2, and M-SZ-3 may not be able to clarify their BA acid strength unambiguously. The J-coupling constants (J_{P-H}) of adsorbed TMP on the BA site (TMPH⁺) may also be used to characterize the BA acid strength. As shown in Figure 5b, the peaks near −3.3 ppm are split into two peaks due to the J-coupling [28]. The J_{P-H} of M-SZ-1, M-SZ-2, and M-SZ-3 was measured as 437, 494, and 474 Hz, respectively. Since higher J_{P-H} reflects stronger acid strength [29], the BA acid strength of the three catalysts is in the order of M-SZ-2 > M-SZ-3 > M-SZ-1, which is consistent with the order based on the ³¹P chemical shifts of TMP adsorbed on BA acid sites. As for the BA acid amount, M-SZ-2 is 112 μmol·g⁻¹, which is the highest among the three samples.

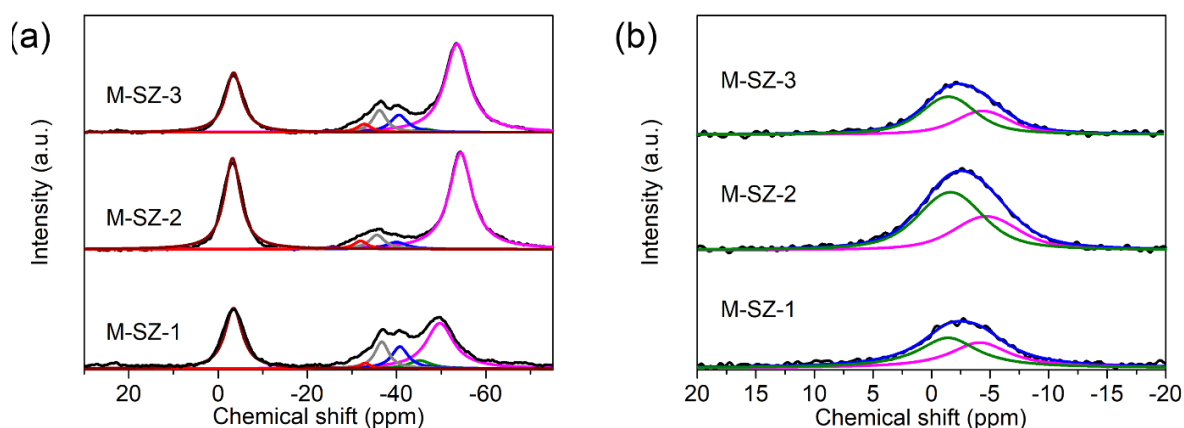


Figure 5. (a) ^1H -decoupled ^{31}P MAS NMR spectra and (b) single-pulse ^{31}P MAS NMR spectra of M-SZ-1, M-SZ-2, and M-SZ-3.

Table 2. The acidity of M-SZ-1, M-SZ-2, and M-SZ-3 acquired from ^{31}P MAS NMR spectra.

Sample	Acid Type	Chemical Shift (ppm)	Acid Amount ($\mu\text{mol}\cdot\text{g}^{-1}$)	$J_{\text{P-H}}$ (Hz)
M-SZ-1	BA	-3.4	68	437
	$\text{LA}_1, \text{LA}_2, \text{LA}_3, \text{LA}_4, \text{LA}_5$	-32.9, -36.7, -40.8, -45.2, -49.7	4, 27, 26, 12, 89	-
M-SZ-2	BA	-3.2	112	494
	$\text{LA}_1, \text{LA}_2, \text{LA}_3, \text{LA}_4, \text{LA}_5$	-31.8, -35.6, -40.5, -, -54.2	9, 19, 12, -, 187	-
M-SZ-3	BA	-3.3	69	474
	$\text{LA}_1, \text{LA}_2, \text{LA}_3, \text{LA}_4, \text{LA}_5$	-32.7, -36.2, -40.6, -46.2, -53.5	9, 22, 22, 4, 157	-

By deconvolution of the peaks attributed to LAs, the LAs of the three catalysts mainly contain five types of LAs, named LA_{1-5} , as shown in Table 2. Among them, LA_4 and LA_5 are related to the original LAs on monoclinic zirconia, and LA_1 , LA_2 , and LA_3 correspond to the sulfate-related LA on the surface of sulfated zirconia [30,31]. By comparing the ^{31}P chemical shifts of TMP adsorbed on LA_1 , LA_2 , and LA_3 shown in Table 2, the orders of the LA_{1-3} acid strength of the three catalysts are also M-SZ-2 > M-SZ-3 > M-SZ-1. However, the ^{31}P chemical shifts of TMP related to LA_{1-3} of the three catalysts are similar, so the differences in LA_{1-3} acid strength are not significant. The LA amounts of three M-SZ are also recorded in Table 2.

3.2. The Isomerization of Butane Catalyzed by M-SZ Catalysts

The isomerization of butane on the three catalysts was monitored by ^{13}C MAS NMR spectroscopy, using $1\text{-}^{13}\text{C}\text{-}n\text{-butane}$ as the reactant. Figure 6 shows the ^{13}C MAS NMR spectra of the catalytic reaction at different times on M-SZ-2. The peak at 13.0 ppm corresponds to the adsorbed $1\text{-}^{13}\text{C}\text{-}n\text{-butane}$, and the peak at 10.5 ppm is assigned to the gaseous $1\text{-}^{13}\text{C}\text{-}n\text{-butane}$ [32]. As the reaction time increases, peaks at 25.0 and 23.7 ppm appear, corresponding to $2\text{-}^{13}\text{C}\text{-}n\text{-butane}$ and $^{13}\text{C}\text{-isobutane}$ ($1\text{-}^{13}\text{C}\text{-isobutane}$ and $2\text{-}^{13}\text{C}\text{-isobutane}$), respectively. The by-product $^{13}\text{C}\text{-isopentane}$ related to the peak at 21.6 ppm may be observed at 10 min, and a new peak at 15.2 ppm corresponding to $^{13}\text{C}\text{-propane}$ appears at 60 min. The results of the catalytic reaction on different M-SZ catalysts at 433 K for 60 min are shown in Table 3, which shows that M-SZ-2 has the highest catalytic performance.

The distributions of reactants and products in the butane isomerization reaction catalyzed by M-SZ-2 at 393, 413, and 433 K are shown in Figure 7. According to the Langmuir Hinshelwood rate equation for the reversible first-order surface reaction [33,34], the rate of butane isomerization is [22,35]:

$$r = \frac{kK_{n\text{C}_4}(P_{n\text{C}_4} - K_{i\text{C}_4}P_{i\text{C}_4}/K_{n\text{C}_4}K_{\text{eq}})}{(1 + K_{n\text{C}_4}P_{n\text{C}_4} + K_{i\text{C}_4}P_{i\text{C}_4})} \quad (1)$$

where k is the reaction rate constant, P_{nC_4} and P_{iC_4} are the partial pressure of n -butane and isobutane, K_{nC_4} and K_{iC_4} are the adsorption equilibrium constant of n -butane and isobutane, respectively, and K_{eq} is the reaction equilibrium constant.

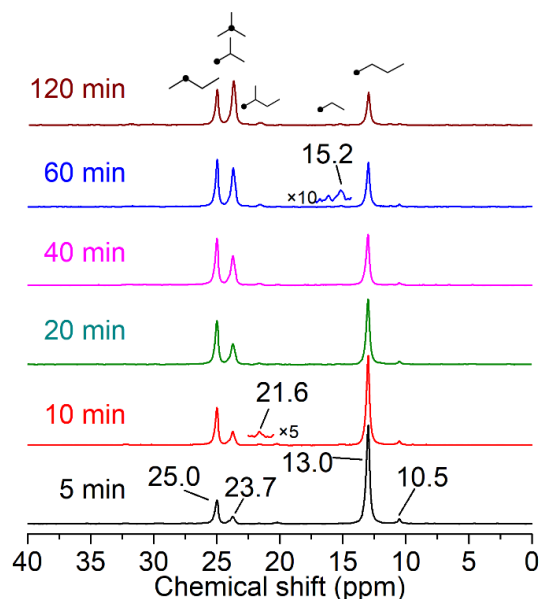


Figure 6. ^{13}C MAS NMR spectra of $1\text{-}^{13}\text{C}$ - n -butane reacted at 433 K with M-SZ-2 as the catalyst at different times.

Table 3. The conversion and product distribution of the butane isomerization at 433 K for 60 min.

Catalysts	X_{60} (%)	$2\text{-}^{13}\text{C}$ - n -Butane (%)	^{13}C -Isobutane (%)
M-SZ-1	0	0	0
M-SZ-2	69.2	28.7	29.5
M-SZ-3	35.0	21.4	10.1

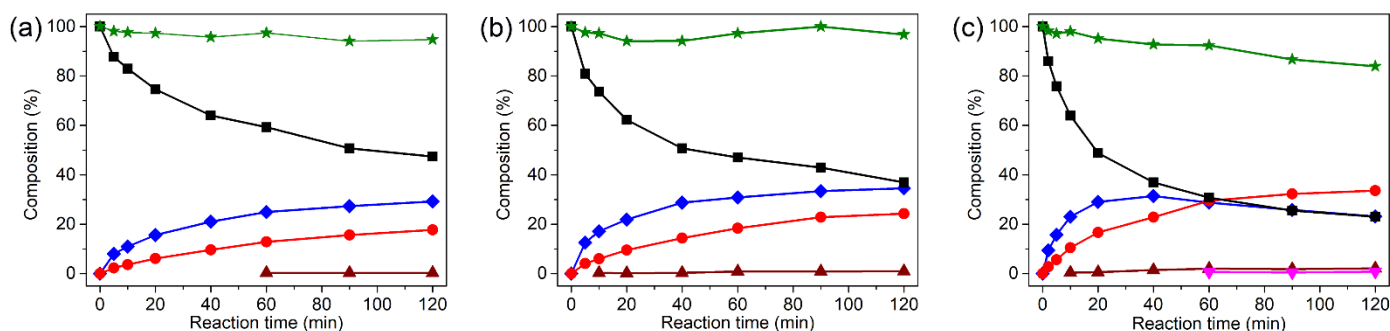


Figure 7. Butane isomerization catalyzed by M-SZ-2 at (a) 393 K, (b) 413 K, and (c) 433 K. (■) $1\text{-}^{13}\text{C}$ - n -butane, (◆) $2\text{-}^{13}\text{C}$ - n -butane, (●) $1\text{-}^{13}\text{C}$ -isobutane and $2\text{-}^{13}\text{C}$ -isobutane, (▲) ^{13}C -isopentane, (▼) ^{13}C -propane, and (★) the total amount of ^{13}C -labeled species.

At relatively low pressure, it is acceptable to suppose $K_{nC_4} = K_{iC_4}$ and $K_{nC_4}(P_{nC_4} + P_{iC_4}) \ll 1$, and Equation (1) can be converted to:

$$-\ln \left[1 - \left(1 + \frac{1}{K_{eq}} \right) \frac{P_{iC_4}}{P_{total}} \right] = kK_{nC_4} \left(1 + \frac{1}{K_{eq}} \right) t \quad (2)$$

By plotting $-\ln [1 - (1 + 1/K_{eq})P_{iC_4}/P_{total}] / (1 + 1/K_{eq})$ against the reaction time (t), Figure 8a with a good linear relationship was obtained, indicating that the catalytic re-

action is mainly through a single molecule mechanism at 393~433 K. The rate constant of butane isomerization catalyzed by M-SZ-2 at 393~433 K may be obtained from the slope in Figure 8a and is shown in Table 4. Further plotting $\ln(kKnC_4)$ against $1000/T$ to obtain Figure 8b, the activation energy (E_a) of the M-SZ-2 catalyst for catalyzing butane isomerization can be calculated as $52.8 \text{ kJ}\cdot\text{mol}^{-1}$. Hsu et al. studied the activation energies of butane isomerization catalyzed by sulfated zirconia, which was $44.8 \text{ kJ}\cdot\text{mol}^{-1}$ [36]. Ma et al. obtained the E_a of butane isomerization catalyzed by sulfated tetragonal zirconia as $45.6 \text{ kJ}\cdot\text{mol}^{-1}$ [34], and Na et al. obtained the E_a of butane isomerization catalyzed by $\text{Cs}_{2.5}\text{H}_{0.5}\text{PW}_{12}\text{O}_{40}$ as $59 \text{ kJ}\cdot\text{mol}^{-1}$ [37]. The E_a of M-SZ-2 is close to the literature results above, indicating that M-SZ-2 also has a high acidic catalytic ability.

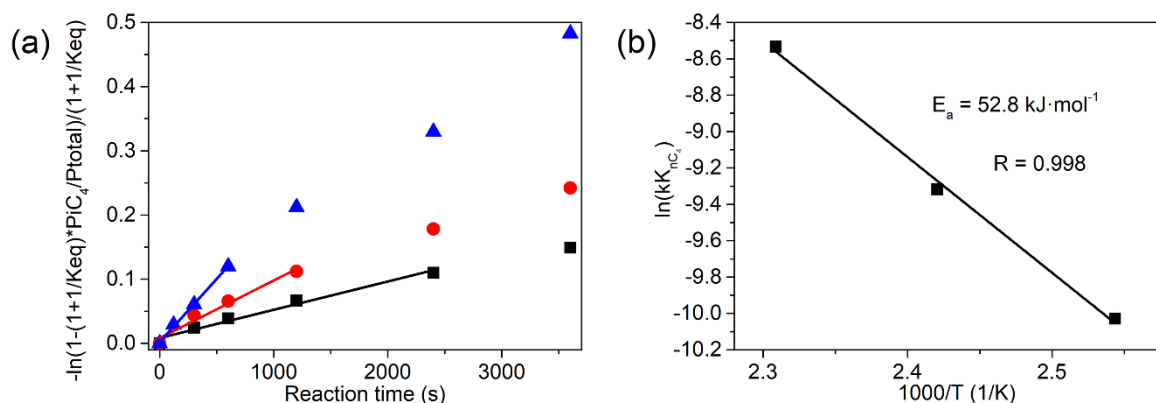


Figure 8. The kinetic study of butane isomerization at different temperatures catalyzed by M-SZ-2. (a) $-\ln[1 - (1 + 1/K_{eq})P_{iC_4}/P_{total}]/(1 + 1/K_{eq})$ vs. reaction time at (■) 393 K, (●) 413 K, and (▲) 433 K, and (b) $\ln(kKnC_4)$ vs. $1000/T$.

Table 4. The kinetic constants of butane isomerization catalyzed by M-SZ-2 at 393 ~ 433 K.

Reaction Temperature (K)	$kKnC_4 \times 10^5 \text{ (mol}\cdot\text{g}^{-1}\cdot\text{s}^{-1})$	R
393	4.41	0.990
413	8.98	0.986
433	19.66	0.998

The results of butane isomerization on M-SZ-1 and M-SZ-3 are shown in Figures S3 and S4. Figures S5 and S6 and Tables S1 and S2 show their corresponding kinetic results. The activation energies of butane isomerization of M-SZ-1 and M-SZ-3 are 148 and $83.8 \text{ kJ}\cdot\text{mol}^{-1}$, respectively.

According to the acidity (Table 2) and E_a results of M-SZ-1, M-SZ-2, and M-SZ-3, it can be found that the E_a of M-SZ catalysts in butane isomerization has a weak correlation with BA acid amount, LA acid amount, and LA acid strength. Nevertheless, E_a is strongly related to the BA acid strength, particularly the J_{P-H} of M-SZ-1, M-SZ-2, and M-SZ-3, which means the BA acid strength is one important factor that influences the butane isomerization. To further prove this inference, the M-SZ-4 catalyst was prepared through sulfation of M-ZrO₂-2 with 2 M H₂SO₄ solution. Its characterization results in Figure S7 showed that M-SZ-4 has the same XRD pattern as that of M-SZ-2, and the J_{P-H} value of M-SZ-4 obtained from ³¹P MAS NMR with TMP probe is 567 Hz, which is higher than the J_{P-H} value of M-SZ-2 (494 Hz). This result shows that M-SZ-4 has stronger BA acid strength than M-SZ-2. The catalytic performance of M-SZ-4 is shown in Figure S8. From the kinetic study in Figure S9 and Table S3, the activation energy of M-SZ-4 is $46.4 \text{ kJ}\cdot\text{mol}^{-1}$. Therefore, the catalytic butane isomerization performance and the BA strength of M-SZ-4 further prove the stronger the BA strength, the lower the activation energy of butane isomerization.

3.3. The Stability of M-SZ and T-SZ Catalysts Operated at High Temperature

According to the literature results, the catalytic performance of butane isomerization over most sulfated tetragonal zirconia decreased with the increase in reaction time [38–40]. In order to compare the thermal stability of sulfated monoclinic zirconia and tetragonal zirconia catalysts, M-SZ-2 and T-SZ-general were calcined at 673 K for 240 h and the catalysts before and after calcination were used to catalyze butane isomerization. The results are shown in Table 5. The conversion of 1-¹³C-*n*-butane and the yield to isobutane on M-SZ-2 only decrease by 7.8% and 12.9% after calcination, respectively. Although T-SZ-general has higher catalytic activity for catalyzing butane isomerization, after calcination at 673 K for 240 h, the conversion of 1-¹³C-*n*-butane and the yield to isobutane decreases by 17.8% and 30.9%, respectively. The results show that M-SZ-2 exhibits higher catalytic stability than T-SZ-general. The XRD patterns of M-SZ-2 and T-SZ-general samples are shown in Figure S10. It can be easily found that calcination at 673 K could result in the phase change of tetragonal zirconia and its sulfated zirconia, while the monoclinic zirconia and its sulfated zirconia remain unchanged.

Table 5. Comparison of the butane isomerization catalyzed by M-SZ-2 and T-SZ-general before and after calcination at 673 K for 240 h at different reaction temperatures for 60 min.

Catalysts	Reaction Temperature (K)	Uncalcined		Calcined at 673 K for 240 h	
		X ₆₀ (%)	Isobutane (%)	X ₆₀ (%)	Isobutane (%)
M-SZ-2	433	69.2	29.5	63.8	25.7
T-SZ-general	338	61.1	32.7	50.2	22.6

4. Conclusions

Monoclinic-phase zirconia samples (M-ZrO₂-1, M-ZrO₂-2, and M-ZrO₂-3) were synthesized and further sulfated to obtain sulfated monoclinic zirconia catalysts (M-SZ-1, M-SZ-2, M-SZ-3, and M-SZ-4). The acidity of monoclinic zirconia and M-SZ samples was thoroughly characterized by ³¹P MAS NMR with TMP probe. Among the acidic properties, including acid type, acid amounts, and acid strength, the BA acid strength plays an important role in catalyzing butane isomerization, i.e., the stronger the BA acid strength, the better the catalytic performance and the lower the activation energy. M-SZ-4 with the strongest Brønsted acidity shows the highest catalytic performance, with its activation energy of 46.4 kJ mol⁻¹, which is close to that of sulfated tetragonal zirconia. The stability tests exhibited that sulfated monoclinic zirconia has better thermal stability than sulfated tetragonal zirconia although sulfated tetragonal zirconia has relatively higher activity. This study may light a way to explore strong solid acid catalysts with high thermal stability operated at relatively high temperatures.

Supplementary Materials: The following are available online at <https://www.mdpi.com/article/10.3390/pr10122693/s1>, Figure S1: The XRD patterns of zirconia synthesized at (a) 393 K, (b) 433 K, and (c) 473 K with different Zr:Urea molar ratio. Figure S2: Instruments for the sample treatment and reaction. Figure S3: Butane isomerization catalyzed by M-SZ-1 at (a) 493 K, (b) 513 K and (c) 533 K. Figure S4: Butane isomerization catalyzed by M-SZ-3 at (d) 433 K, (e) 453 K and (f) 473 K. Figure S5: The kinetic study of butane isomerization at different temperatures catalyzed by M-SZ-1. Figure S6: The kinetic study of butane isomerization at different temperatures catalyzed by M-SZ-3. Figure S7: (a) XRD patterns of M-SZ-2 and M-SZ-4, (b) ³¹P MAS NMR spectrum of M-SZ-4. Figure S8: Butane isomerization catalyzed by M-SZ-4 at (a) 373 K, (b) 413 K, and (c) 433 K. Figure S9: The kinetic study of butane isomerization at different temperatures catalyzed by M-SZ-4. Figure S10: The XRD patterns of (a) T-ZrO₂-general, (b) T-SZ-general, (c) M-ZrO₂-2, and (d) M-SZ-2 calcined in air at 673 K for different times. Table S1: The kinetic constants of butane isomerization catalyzed by M-SZ-1 at 493–533 K. Table S2: The kinetic constants of butane isomerization catalyzed by M-SZ-3 at 433–473 K. Table S3: The kinetic constants of butane isomerization catalyzed by M-SZ-4 at 373–433 K.

Author Contributions: Methodology, D.H., B.Y. and H.H.; Conceptualization, B.Y. and H.H.; Data curation, D.H.; Formal analysis, D.H., W.F., B.Y. and H.H.; Investigation, D.H.; Project administration, H.H.; Writing—original draft, D.H.; Supervision, L.Z., B.Y. and H.H.; Funding acquisition, H.H.;

Writing—review and editing, D.H., W.F., L.Z., B.Y. and H.H. All authors have read and agreed to the published version of the manuscript.

Funding: This research was supported by the National Natural Science Foundation of China (22088101), the Ministry of Science and Technology (2022YFA1503504), and SINOPEC (420068-2).

Conflicts of Interest: The authors declare no conflict of interest.

References

1. Wang, P.Z.; Yue, Y.Y.; Wang, T.H.; Bao, X.J. Alkane isomerization over sulfated zirconia solid acid system. *Int. J. Energy Res.* **2020**, *44*, 3270–3294. [[CrossRef](#)]
2. Potter, M.E.; Le Brocq, J.J.M.; Oakley, A.E.; McShane, E.B.; Vandegehuchte, B.D.; Raja, R. Butane isomerization as a diagnostic tool in the rational design of solid acid catalysts. *Catalysts* **2020**, *10*, 1099. [[CrossRef](#)]
3. Echevskii, G.V.; Aksenov, D.G.; Kodenev, E.G.; Ovchinnikova, E.V.; Chumachenko, V.A. Activity of a sulfated zirconia catalyst in isomerization of *n*-butane fractions. *Pet. Chem.* **2019**, *59*, S101–S107. [[CrossRef](#)]
4. Villegas, J.I.; Kumar, N.; Heikkila, T.; Smieskova, A.; Hudec, P.; Salmi, A.; Murzin, D.Y. A highly stable and selective Pt-modified mordenite catalyst for the skeletal isomerization of *n*-butane. *Appl. Catal. A Gen.* **2005**, *284*, 223–230. [[CrossRef](#)]
5. Yadav, G.D.; Nair, J.J. Sulfated zirconia and its modified versions as promising catalysts for industrial processes. *Microporous Mesoporous Mater.* **1999**, *33*, 1–48. [[CrossRef](#)]
6. Song, X.M.; Sayari, A. Sulfated zirconia-based strong solid-acid catalysts: Recent progress. *Catal. Rev. Sci. Eng.* **1996**, *38*, 329–412. [[CrossRef](#)]
7. Adeeva, V.; Liu, H.Y.; Xu, B.Q.; Sachtler, W.M.H. Alkane isomerization over sulfated zirconia and other solid acids. *Top. Catal.* **1998**, *6*, 61–76. [[CrossRef](#)]
8. Yamaguchi, T. Alkane isomerization and acidity assessment on sulfated ZrO₂. *Appl. Catal. A Gen.* **2001**, *222*, 237–246. [[CrossRef](#)]
9. Morterra, C.; Cerrato, G.; Pinna, F.; Signoreto, M. Crystal phase, spectral features, and catalytic activity of sulfate-doped zirconia systems. *J. Catal.* **1995**, *157*, 109–123. [[CrossRef](#)]
10. Comelli, R.A.; Vera, C.R.; Parera, J.M. Influence of ZrO₂ crystalline-structure and sulfate ion concentration on the catalytic activity of SO₄²⁻-ZrO₂. *J. Catal.* **1995**, *151*, 96–101. [[CrossRef](#)]
11. Stichert, W.; Schuth, F. Synthesis of catalytically active high surface area monoclinic sulfated zirconia. *J. Catal.* **1998**, *174*, 242–245. [[CrossRef](#)]
12. Stichert, W.; Schüth, F.; Kuba, S.; Knözinger, H. Monoclinic and tetragonal high surface area sulfated zirconias in butane isomerization: CO adsorption and catalytic results. *J. Catal.* **2001**, *198*, 277–285. [[CrossRef](#)]
13. Zhang, X.G.; Rabee, A.I.M.; Isaacs, M.; Lee, A.F.; Wilson, K. Sulfated zirconia catalysts for D-sorbitol cascade cyclodehydration to isosorbide: Impact of zirconia phase. *ACS Sustain. Chem. Eng.* **2018**, *6*, 14704–14712. [[CrossRef](#)]
14. Shukla, S.; Seal, S. Mechanisms of room temperature metastable tetragonal phase stabilisation in zirconia. *Int. Mater. Rev.* **2005**, *50*, 45–64. [[CrossRef](#)]
15. Morales, M.D.; Infantes-Molina, A.; Lázaro-Martínez, J.M.; Romanelli, G.P.; Pizzio, L.R.; Rodríguez-Castellón, E. Heterogeneous acid catalysts prepared by immobilization of H₃PW₁₂O₄₀ on silica through impregnation and inclusion, applied to the synthesis of 3H-1,5-benzodiazepines. *Mol. Catal.* **2020**, *485*, 110842. [[CrossRef](#)]
16. Yu, H.G.; Fang, H.J.; Zhang, H.L.; Li, B.J.; Deng, F. Acidity of sulfated tin oxide and sulfated zirconia: A view from solid-state NMR spectroscopy. *Catal. Commun.* **2009**, *10*, 920–924. [[CrossRef](#)]
17. Zheng, A.M.; Liu, S.B.; Deng, F. ³¹P NMR chemical shifts of phosphorus probes as reliable and practical acidity scales for solid and liquid catalysts. *Chem. Rev.* **2017**, *117*, 12475–12531. [[CrossRef](#)]
18. Lunsford, J.H.; Sang, H.; Campbell, S.M.; Liang, C.H.; Anthony, R.G. An NMR study of acid sites on sulfated-zirconia catalysts using trimethylphosphine as a probe. *Catal. Lett.* **1994**, *27*, 305–314. [[CrossRef](#)]
19. Barich, D.H.; Nicholas, J.B.; Xu, T.; Haw, J.F. Theoretical and experimental study of the ¹³C chemical shift tensors of acetone complexed with Brønsted and Lewis acids. *J. Am. Chem. Soc.* **1998**, *120*, 12342–12350. [[CrossRef](#)]
20. Hunger, M. Multinuclear solid-state NMR studies of acidic and non-acidic hydroxyl protons in zeolites. *Solid State Nucl. Magn. Reson.* **1996**, *6*, 1–29. [[CrossRef](#)]
21. Ma, Z.Y.; Yang, C.; Wei, W.; Li, W.H.; Sun, Y.H. Catalytic performance of copper supported on zirconia polymorphs for CO hydrogenation. *J. Mol. Catal. A Chem.* **2005**, *231*, 75–81. [[CrossRef](#)]
22. Zhang, L.; Yue, B.; Ren, Y.H.; Chen, X.Y.; He, H.Y. An aluminum promoted cesium salt of 12-tungstophosphoric acid: A catalyst for butane isomerization. *Catal. Sci. Technol.* **2013**, *3*, 2113–2118. [[CrossRef](#)]
23. Chuah, G.K.; Jaenicke, S.; Cheong, S.A.; Chan, K.S. The influence of preparation conditions on the surface area of zirconia. *Appl. Catal. A Gen.* **1996**, *145*, 267–284. [[CrossRef](#)]
24. Bianchi, C.L.; Ardizzone, S.; Cappelletti, G. Surface state of sulfated zirconia: The role of the sol-gel reaction parameters. *Surf. Interface Anal.* **2004**, *36*, 745–748. [[CrossRef](#)]
25. Bosman, H.J.M.; Pijpers, A.P.; Jaspers, A. An X-ray photoelectron spectroscopy study of the acidity of SiO₂-ZrO₂ mixed oxides. *J. Catal.* **1996**, *161*, 551–559. [[CrossRef](#)]

26. Fu, Y.Y.; Zhang, L.; Yue, B.; Chen, X.Y.; He, H.Y. Simultaneous characterization of solid acidity and basicity of metal oxide catalysts via the solid-state NMR technique. *J. Phys. Chem. C* **2018**, *122*, 24094–24102. [[CrossRef](#)]
27. Chu, Y.Y.; Yu, Z.W.; Zheng, A.M.; Fang, H.J.; Zhang, H.L.; Huang, S.J.; Liu, S.B.; Deng, F. Acidic strengths of Brønsted and Lewis acid sites in solid acids scaled by ^{31}P NMR chemical shifts of adsorbed trimethylphosphine. *J. Phys. Chem. C* **2011**, *115*, 7660–7667. [[CrossRef](#)]
28. Zhao, B.Y.; Pan, H.J.; Lunsford, J.H. Characterization of $[(\text{CH}_3)_3\text{P-H}]^+$ complexes in normal H-Y, dealuminated H-Y, and H-ZSM-5 zeolites using ^{31}P solid-state NMR spectroscopy. *Langmuir* **1999**, *15*, 2761–2765. [[CrossRef](#)]
29. Lunsford, J.H. Characterization of acidity in zeolites and related oxides using trimethylphosphine as a probe. *Top. Catal.* **1997**, *4*, 91–98. [[CrossRef](#)]
30. Wang, S.; Fang, Y.; Huang, Z.; Xu, H.L.; Shen, W. The effects of the crystalline phase of zirconia on C-O activation and C-C coupling in converting syngas into aromatics. *Catalysts* **2020**, *10*, 262. [[CrossRef](#)]
31. Zhang, H.L.; Yu, H.G.; Zheng, A.M.; Li, S.H.; Shen, W.L.; Deng, F. Reactivity enhancement of 2-propanol photocatalysis on $\text{SO}_4^{2-}/\text{TiO}_2$: Insights from solid-state NMR spectroscopy. *Environ. Sci. Technol.* **2008**, *42*, 5316–5321. [[CrossRef](#)]
32. Chen, B.; Munson, E.J. Investigation of the mechanism of *n*-butane oxidation on vanadium phosphorus oxide catalysts: Evidence from isotopic labeling studies. *J. Am. Chem. Soc.* **2002**, *124*, 1638–1652. [[CrossRef](#)]
33. Zarkalis, A.S.; Hsu, C.Y.; Gates, B.C. Solid superacid catalysis: Kinetics of butane isomerization catalyzed by a sulfated oxide containing iron, manganese, and zirconium. *Catal. Lett.* **1994**, *29*, 235–239. [[CrossRef](#)]
34. Ma, Z.N.; Zou, Y.; Hua, W.M.; He, H.Y.; Gao, Z. In situ ^{13}C MAS NMR study on the mechanism of butane isomerization over catalysts with different acid strength. *Top. Catal.* **2005**, *35*, 141–153. [[CrossRef](#)]
35. Ma, Z.N.; Hua, W.M.; Ren, Y.; He, H.Y.; Gao, Z. *n*-Butane isomerization over Cs-salts of $\text{H}_3\text{PW}_{12}\text{O}_{40}$: A mechanistic study by ^{13}C MAS NMR. *Appl. Catal. A Gen.* **2003**, *256*, 243–250. [[CrossRef](#)]
36. Hsu, C.Y.; Heimbuch, C.R.; Armes, C.T.; Gates, B.C. A highly active solid superacid catalyst for *n*-butane isomerization: A sulfated oxide containing iron manganese and zirconium. *J. Chem. Soc. Chem. Commun.* **1992**, *22*, 1645–1646. [[CrossRef](#)]
37. Na, K.; Okuhara, T.; Misono, M. Skeletal isomerization of *n*-butane over caesium hydrogen salts of 12-tungstophosphoric acid. *J. Chem. Soc. Faraday Trans.* **1995**, *91*, 367–373. [[CrossRef](#)]
38. Sun, Y.Y.; Yuan, L.N.; Ma, S.Q.; Han, Y.; Zhao, L.; Wang, W.; Chen, C.L.; Xiao, F.S. Improved catalytic activity and stability of mesostructured sulfated zirconia by Al promoter. *Appl. Catal. A Gen.* **2004**, *268*, 17–24. [[CrossRef](#)]
39. Wang, J.H.; Mou, C.Y. Alumina-promoted mesoporous sulfated zirconia: A catalyst for *n*-butane isomerization. *Appl. Catal. A Gen.* **2005**, *286*, 128–136. [[CrossRef](#)]
40. Gao, Z.; Xia, Y.D.; Hua, W.M.; Miao, C.X. New catalyst of $\text{SO}_4^{2-}/\text{Al}_2\text{O}_3\text{-ZrO}_2$ for *n*-butane isomerization. *Top. Catal.* **1998**, *6*, 101–106. [[CrossRef](#)]